



HORIZON 2020 RESEARCH AND INNOVATION FRAMEWORK PROGRAMME OF THE EUROPEAN ATOMIC ENERGY COMMUNITY

Nuclear Fission and Radiation Protection 2018 (NFRP-2018-4)

Project acronym: **SANDA**

Project full title: **Solving Challenges in Nuclear Data for the Safety of European Nuclear facilities**

Grant Agreement no.: **H2020 Grant Agreement number: 847552**

Workpackage N°: **WP2**

Identification N°: **D2.13**

Type of document: ***Deliverable***

Title: Report on fission yield studies with FALSTAFF at NFS

Dissemination Level: **PU**

Reference:

Status: **VERSION 2**

Comments:

| | Name | Partner | Date | Signature |
|------------------|-------------|---------|------------|-----------|
| Prepared by: | Diane Doré | | 22-12-2023 | |
| WP leader: | D. Cano-Ott | 1 | 19-06-2024 | |
| IP Co-ordinator: | E. González | 1 | 19-06-2023 | |

SANDA WP2, Subtask 2.5.1.
Report for the Deliverable D2.13
D. DORÉ, J.E. DUCRET, X. LEDOUX, P. MARINI, D. RAMOS ET AL.

Introduction

The goal of the E814 experiment was to study fission fragments of ^{235}U over the large incident neutron energy domain available at NFS. In the framework of WP1, the deliverable 1.3 report [1] consisted in the presentation of the setup improvements and ^{252}Cf results of the FALSTAFF spectrometer. In the report of the milestone 2.3 [2], the completion of the experiment performed with the first arm of FALSTAFF at NFS (SPIRAL2/GANIL, Experiment E814) in Fall 2022 was presented. In the present report, fission yield studies with FALSTAFF at NFS will be presented. The beam and target descriptions and the incident neutron energy distribution have already been presented in [2] report but are presented here again in order to have a complete view of the experiment. In addition, the experimental setup is described, the calibration procedure, the experimental distributions and comparisons with simulations are presented. Since the experiment was achieved only one year ago, results are preliminary.

FALSTAFF spectrometer

The FALSTAFF spectrometer [3] is a two-arm instrument designed to study the evolution of the pre- and post-neutron emission masses of fragments, their kinetic energy and charge according to the excitation energy (E^*) of the fissioning system. This information will permit to study the excitation energy sharing between fragments thanks to the neutron multiplicity that can be deduced from the pre- and post- fragments masses. The evolution of the role of shell effects can be studied through the evolution of mass and charge distribution according to the excitation energy. The deformation at scission will be investigated through the kinetic energy of the fragments.

Experimentally, the goal is to detect both fission fragments in coincidence with two identical arms. Each detection arm is based on two Sed-MWPC detectors [4], start and stop detectors, and an axial ionization chamber (see Fig.1).

Tof detectors

The Sed-MWPC detectors are made up of an emissive foil, an accelerating grid and a MWPC detectors. An aluminized Mylar foil of 0.5 μm thickness, inclined at 45° with respect to the horizontal direction and polarized at -10 kV, is placed along the path of the fission fragments. A grounded grid placed at 1 cm from the emissive foil generates a high electric field close to the foil. The secondary electrons produced by the ion crossing the Mylar foil are then accelerated to 10 keV and fly towards the MWPC detector. The accelerated electrons pass through the MWPC entrance foil (0.9 μm aluminized Mylar) with 70% efficiency. They create ionization electrons inside the gas which are then amplified while drifting towards the cathode. The amplification takes place over the whole drift path due to the low pressure of the gas (4-6Torr). The time signal is then read from the wire plane by a fast amplifier. The spatial information is taken from the charge induced on a 2D pixelized cathode.

These detectors provide information on fission-fragment time-of-flights and positions with resolutions (σ) of 120 ps and 1.2 mm respectively [2]. With this information, the trajectories and then the velocity vectors are reconstructed.

Energy detector

The cylindrical axial ionization chamber has an outside effective diameter of 440 mm and a length of 400 mm. The cathode is the detector entrance window separated to the anode by a distance of 395 mm. A potential of -8 kV is applied to the cathode while the readout electrode is the grounded anode. The entrance window is a Mylar foil 0.9 μm thick with a diameter of 232 mm. To polarize the Mylar foil and to ensure a good electrical conductivity, 50 nm of aluminum

are deposited on each side. In order to avoid strong mechanical tension, the entrance window is maintained by a grid of 12 nylon wires, 6 vertical and 6 horizontal. These wires have a diameter of 350 microns. The electric field uniformity is assured by 38 aluminum rings, 270 mm in diameter, spaced out by 10 mm and interconnected by a 10 MW resistance allowing to maintain a uniform field along the chamber. A Frisch grid is installed in front of the anode to ensure the shielding its shielding from the influence of the charges moving in the ionization region. An electronic signal is induced to the anode only once the electrons have crossed the grid. The ionizing gas is isobutane at a pressure between 20 and 30 Torr flowing at of 1.5 L/h. The ionization chamber measures the residual energy through the longitudinal profile of the energy loss of each fission-fragment with a resolution of ~1% [2].

Thanks to energy and velocity measurements and after energy loss corrections, the fragment mass is reconstructed. Previous simulations taking into account the full geometry and experimental resolutions showed that the pre- and post-fragment masses can be determined with resolutions of ~1 amu and ~2 amu respectively.

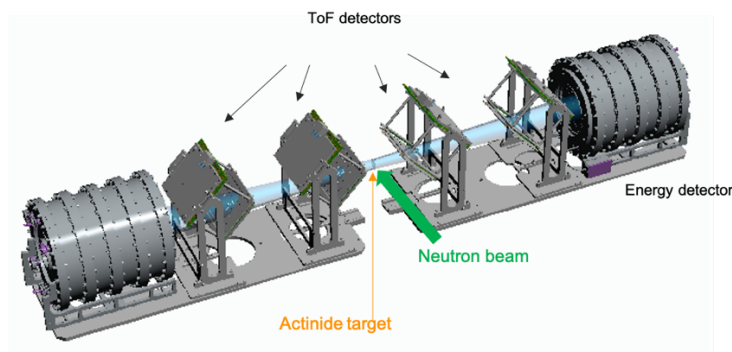


Fig. 1. Sketch of the Falstaff spectrometer

In its final version (the second arm being in construction), FALSTAFF will provide information on these pre- and post- neutron evaporation fragment masses. However, the E814_20 experiment at NFS [5] was performed with one arm of the spectrometer. In this case, velocity and energy measurements allow us to reconstruct the post-evaporation fragment masses.

Neutron beam and FALSTAFF target

The white neutron spectrum produced by deuterons stopped in a thick ${}^9\text{Be}$ target in the NFS converter room was used to perform the experiment. The ${}^{235}\text{U}$ target provided by JRC-Geel is a disk of radius 2.8 cm with a thickness of 195 $\mu\text{g}/\text{cm}^2$. The beam impacts the target perpendicularly to the thin edge of the disk allowing to minimize the material crossed by the fragments. An image obtained with a photostimulable phosphor plate placed at the exit of the Falstaff chamber showed that the target was well positioned at the center of the beam spot.

In order to determine the neutron energy producing the fission detected by FALSTAFF, two LaBr₃ gamma detectors have been added close to the target. They gave an absolute time reference by detecting the gamma flash produced by deuterons on Be in the converter room, allowing thus for an absolute determination, event by event, of the time of flight of the neutron which triggers the fission reaction detected in FALSTAFF. The incident neutron flux deduced from the fission counting rate in FALSTAFF have been compared to the beam flux obtained with different methods (Fig.2). The agreement is rather good and confirms the FALSTAFF efficiency calculations (~0.5 %).

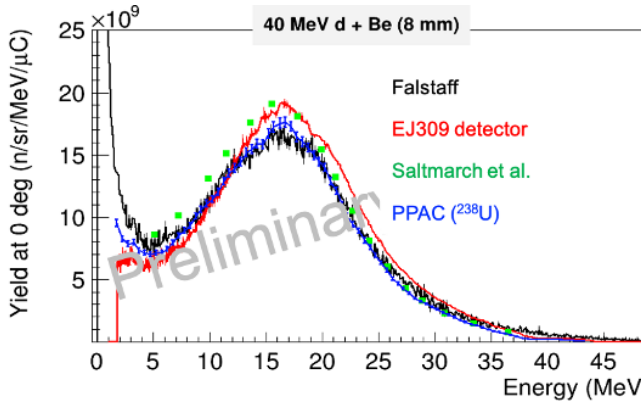


Fig. 2. Incident neutron flux at NFS for the ^{235}U FALSTAFF experiment compared with other measurements.

Acquisition and trigger

The acquisition is based on two different systems:

- the cathodes pad/strips signal from the start and stop detectors are digitized using the GET acquisition system [6] on a μTCA crate,
- all others signal (timing information from start and stop detectors, anode and grid signal from the axial ionization chamber) are acquired by using the standard GANIL acquisition based on a VME crate.

The trigger is made by the coincidence between start and stop detectors. For the analysis, a condition is applied on all data to keep only fragments by rejecting alpha (small amplitude signals in the ionization chamber). An additional condition (velocity > 0) is mandatory to reject events coming from the californium contamination on the emissive foil (technical problem solved since the experiment) of the stop detector. Experimentally, a condition is also applied on the reconstructed point on the source/target.

Energy and time calibration

The calibration is a delicate point for this kind of experiment. We adopted the well-known method by using experimentally a ^{252}Cf source and the associated simulation. This one use GEF [7] results as input of a GEANT4 [8] in which the full geometry of the experimental setup is implemented. GEF code is chosen since it is possible to use it also for ^{235}U data. In Fig.3 the calibrated experimental and simulated residual energy distributions in the ionization chamber are compared. It has been found that an additional condition on the angle is necessary to obtain the good ratio between heavy and light fragment.

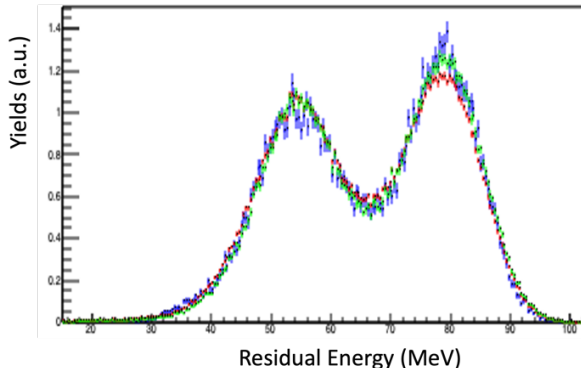


Fig. 3. ^{252}Cf residual energy (MeV) distributions: experimental results without conditions on angle in red, with angle condition in green (experimental) and blue (simulations).

Integral of the distributions are normalized to the 100.

Indeed, for some fragments the angle is too large and do not lose all their energy in the gas of the ionization chamber but they hit the surrounding. With the condition on the polar angle ($\theta < 4^\circ$) experimental and simulated data show a good agreement. Corrections to apply to the residual energy in order to recover the full statistics (without angle condition) is under study.

The time is obtained via the anode signal of the Sed-MWPC passed through a constant fraction discriminator and a time-to-digital converter. The acquisition card is calibrated with a time calibrator. A finer adjustment was applied by comparing experimental results and simulation. Fig. 4 shows the experimental and simulated Time-of-Flight (TOF) distributions after calibrations. Here we observe that the experimental distribution extends a bit towards smaller time-of-flights.

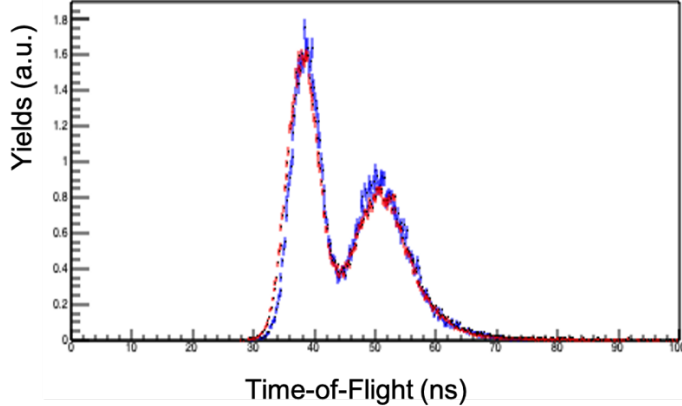


Fig.4. ^{252}Cf experimental (red) and simulated (blue) Time-of-Flight distributions.
Integral of the distributions are normalized to 100.

^{235}U Experimental distributions

For the E814_20 experiment, the white NFS neutron beam spectrum extended from 0.5 MeV up to 40 MeV. The neutron flux was around 1.6×10^{10} n/sr/MeV/ μC at 15 MeV. The beam impinged on the side of a $^{235}\text{UF}_4$ target of 195 $\mu\text{g}/\text{cm}^2$ thick provided by JRC-Geel. The neutron energy spectrum deduced from FALSTAFF is in agreement with other experiments performed at NFS [2]. In Fig.5 the fragment residual energy and velocity distributions are shown. As expected, these spectra are slightly different from those of ^{252}Cf .

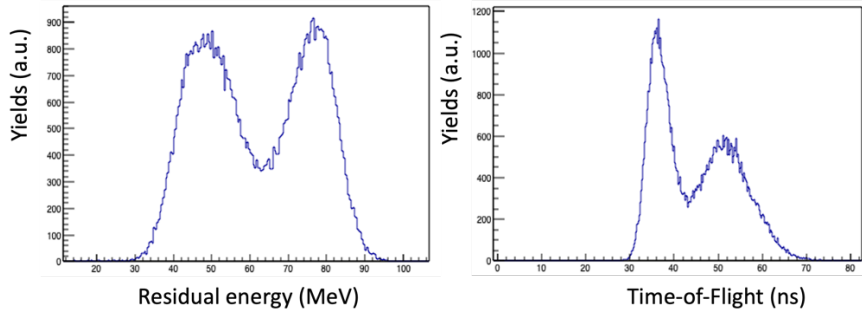


Fig 5. ^{235}U experimental residual energy and time of flight distributions summed over the whole NFS energy spectra.

The ^{235}U fission observables have then been studied according to the neutron energy. Although events over the entire range of incident neutron energies were registered during the experiment, in this report we focus on energies lower than 20 MeV. In Fig. 6 red curves show the experimental residual energy for different incident energy bins. The fragment energy bin width is 1 MeV while the incident neutron energy bin width was 2 MeV (± 1 MeV around the central values indicated in Fig. 6). As expected, we see an asymmetric distribution for all energies. We note that the valley is slowly filling-up when the excitation energy i.e., the neutron energy increases. We also remark that the ratio between the light fragment yield (high energy) and the heavy fragment peak (low energy) varies according to the incident neutron energy. Comparisons with simulated data will be done in the next sections. Distributions for higher incident neutron energy have also been obtained, but some corrections have to be applied and it is still under investigation.

In order to calculate the mass, corrections have to be applied to the residual energy measured in the ionization chamber to take into account energy losses in the entrance window and also in the emissive foil of the stop detector. In this way we obtain the energy and the velocity at the same point in the detection system, that's to say between the start and stop detectors. The charge and the mass of the fragment are determined in an iterative procedure. First, the mass is set to the value obtain with the velocity and the un-corrected energy. Here the charge is given by the UCD (Unchanged Charge Density) prescription. Then, an iterative procedure is applied where the energy, the mass and the charge are calculated after each correction step. The energy loss table of DPASS (normalized with a factor 1.1) is used in GEANT4 and in the data analysis. Details can be found in [9].

Fig. 7 presents the result of the procedure for different excitation energy bins. The mass bin width is 2 u.m.a while the incident neutron energy bin width was 2 MeV. Here again the valley is slowly filled with increasing excitation energy. The width of the heavy fragment distribution seems large. One note that the ratio of the peaks does not vary as much as in the energy distributions. Results are also presented in Tables A, B and C at the end of the document.

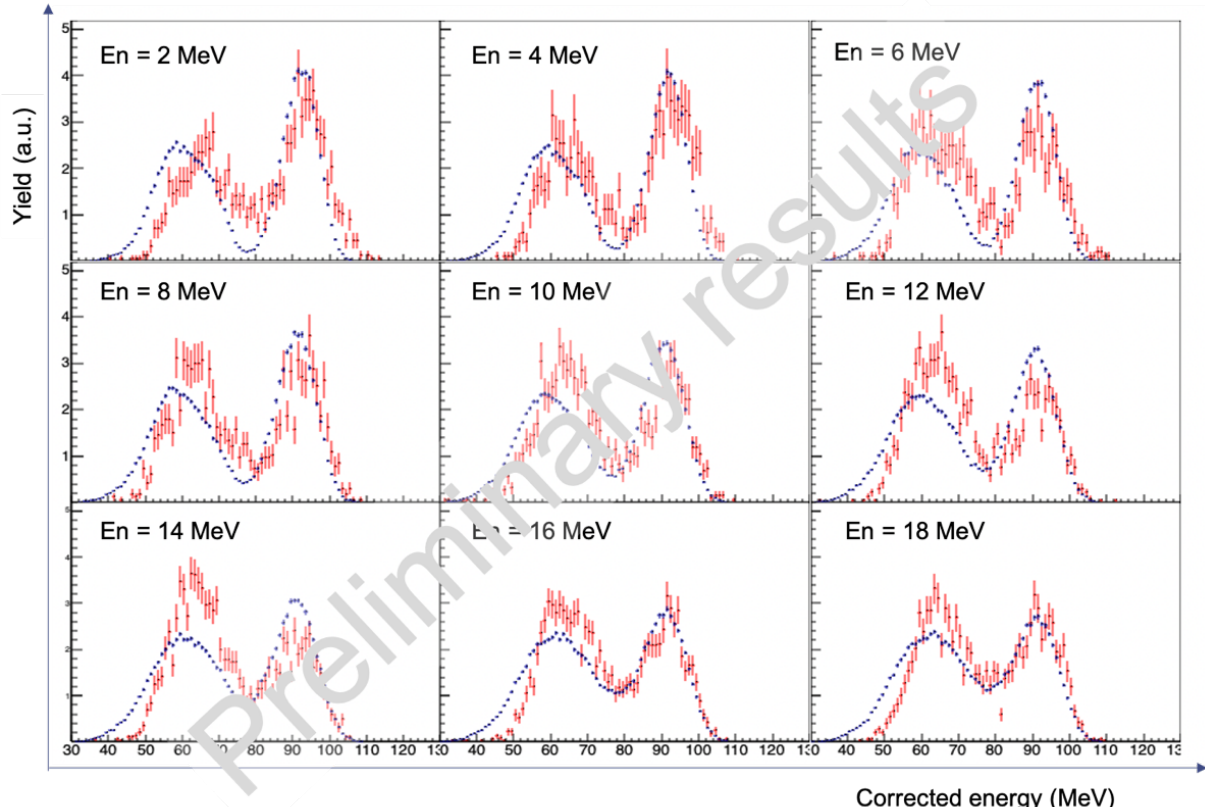


Fig.6. Experimental and simulated residual energy distributions for different incident energy bins.

Comparisons with simulations

Experimental results were compared to those of GEF [7]. GEF was run for each incident neutron energy. As in the case of ^{252}Cf , GEF results were used as input of a GEANT4 simulation in which the FALSTAFF geometry was implemented in great details. Experimental resolutions are also included in the simulations. Results, in blue, are compared to FALSTAFF data in Fig. 6 and 7. Integral of the curves are normalized to 100. The general trends are the same for data and simulations over the incident neutron energy range.

In Fig. 6 we observe that the light fragment peak is located at the same place and has almost the same width in data and simulation. For the heavy fragment, data are peaked at an energy slightly higher than computed with the simulation. In addition, the experimental widths are smaller than the simulated ones. This unexpected discrepancy is still under investigation.

In Fig. 7 the agreement between data and simulations remains good for light fragments over the whole range of neutron energy, but for the heavy fragment there are some discrepancies. The experimental heavy fragment peak is at larger mass and has a larger width than the simulations. The larger mass comes from the higher residual energy. However, the larger width is in contradiction with the smaller one observed in Fig.6. This feature, in addition to the one observed in Fig.6, implies that we have to investigate further both the data analysis and the simulation.

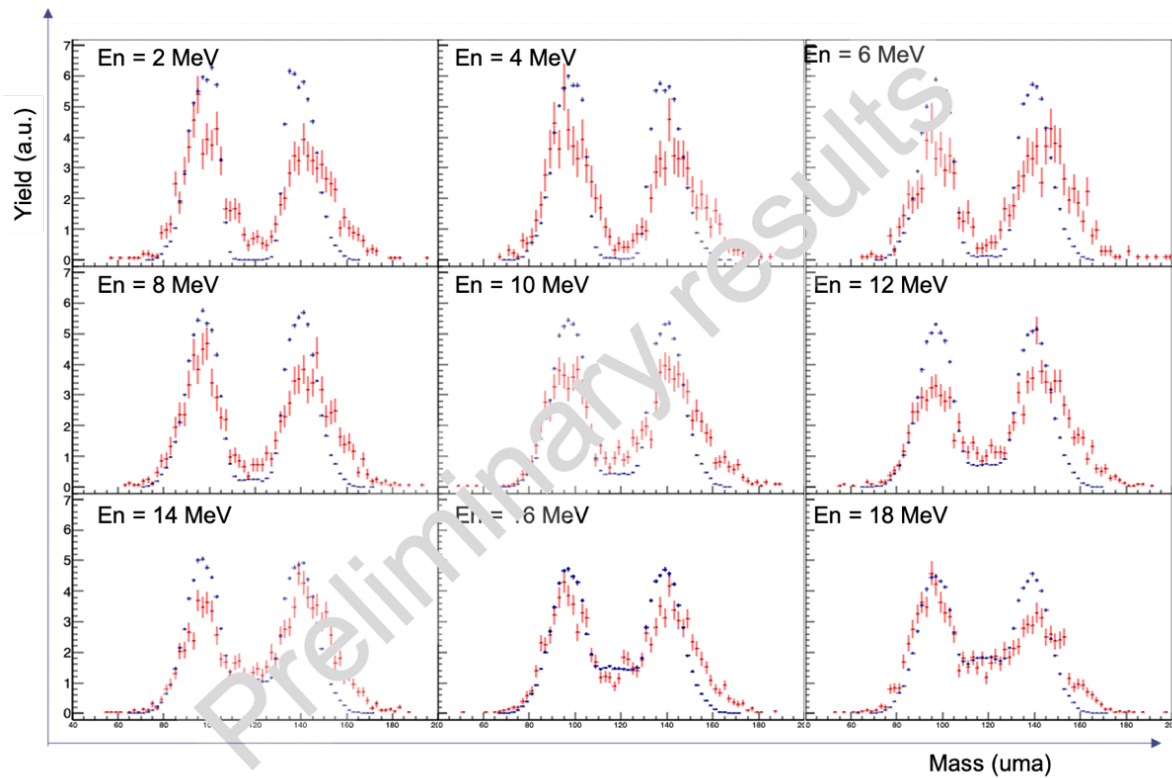


Fig.7. Experimental and simulated fragment mass distributions for different incident energy bins.
Integral of the distributions are normalized 100.

Conclusion

The E814 experiment conducted at NFS in November and December 2022 was performed without major problem but with a total number of events smaller than expected. Preliminary results are encouraging even if there are some points to investigate. The analysis is still in progress and we plan to submit a paper before summer 2024. We are in contact with M. Otsuka and, after publication, results will be included in EXFOR. We also collaborate with our colleagues developing the FIFRELIN deexcitation

code [10]. With the 2-arms FALSTAFF setup, the pre-fragment mass distributions will be used to settle FIFRELIN parameters. However, since FIFRELIN can use GEF data as pre-neutron data, it will be possible to compare FALSTAFF and FIFRELIN post-fragment masses soon.

The second arm of FALSTAFF is in construction and an experiment with the full setup will be submitted in Fall 2024 in order to perform the experiment in 2025.

References

- [1] D. Doré et al., Report (D1.3) on the performances of new devices for precise study of fission products and their decay in view of measurements, March 2022
- [2] D. Doré et al., Report (M2.3) on the completion of the measurements with FALSTAFF at NFS. June 2023
- [3] D. Doré et al., Nuclear Data Sheets 119, 346 (2014).
- [4] J. Pancin et al. J. Instrum., 4 (2009) P12012.
- [5] X. Ledoux et al., EPJ A (2021) 57:257.
- [6] E. Pollacco et al., NIM A887 (2018) 81-93.
- [7] K.H. Schmidt et al., Technical report, JEFF Report 24, 014.
- [8] J. Allison et al., Nucl. Instrum. Meth. A 835 (2016) 186-225.
- [9] T. Materna et al., NIM B 505 (2021) 1-16.
- [10] O. Litaize et al., EPJA 51 (2015) 177.

Tab. A Preliminary ^{235}U mass yields for incident neutron energies of 2,4 and 6 MeV.
See text for details.

| Energy (MeV) | En = 2 MeV | | En = 4 MeV | | En = 6 MeV | |
|-----------------|---------------|--------|---------------|--------|---------------|--------|
| | Yields (a.u.) | Errors | Yields (a.u.) | Errors | Yields (a.u.) | Errors |
| 67 | 0,07 | 0,07 | 0,11 | 0,11 | 0,10 | 0,10 |
| 69 | 0,14 | 0,10 | 0,00 | 0,00 | 0,10 | 0,10 |
| 71 | 0,07 | 0,07 | 0,11 | 0,11 | 0,29 | 0,17 |
| 73 | 0,28 | 0,14 | 0,32 | 0,18 | 0,00 | 0,00 |
| 75 | 0,14 | 0,10 | 0,11 | 0,11 | 0,10 | 0,10 |
| 77 | 0,07 | 0,07 | 0,53 | 0,24 | 0,49 | 0,22 |
| 79 | 0,48 | 0,18 | 0,32 | 0,18 | 0,39 | 0,19 |
| 81 | 0,97 | 0,26 | 0,53 | 0,24 | 0,49 | 0,22 |
| 83 | 0,90 | 0,25 | 1,16 | 0,35 | 1,66 | 0,40 |
| 85 | 2,21 | 0,39 | 1,80 | 0,44 | 1,46 | 0,38 |
| 87 | 1,93 | 0,37 | 2,01 | 0,46 | 2,04 | 0,45 |
| 89 | 2,21 | 0,39 | 3,28 | 0,59 | 2,04 | 0,45 |
| 91 | 3,31 | 0,48 | 4,02 | 0,65 | 1,85 | 0,42 |
| 93 | 3,80 | 0,51 | 3,60 | 0,62 | 3,12 | 0,55 |
| 95 | 4,97 | 0,59 | 4,87 | 0,72 | 4,48 | 0,66 |
| 97 | 4,63 | 0,57 | 4,76 | 0,71 | 3,60 | 0,59 |
| 99 | 3,73 | 0,51 | 4,13 | 0,66 | 3,80 | 0,61 |
| 101 | 3,66 | 0,50 | 3,17 | 0,58 | 3,60 | 0,59 |
| 103 | 4,77 | 0,57 | 3,81 | 0,63 | 3,12 | 0,55 |
| 105 | 3,04 | 0,46 | 3,17 | 0,58 | 2,73 | 0,52 |
| 107 | 2,42 | 0,41 | 3,17 | 0,58 | 2,24 | 0,47 |
| 109 | 1,93 | 0,37 | 2,33 | 0,50 | 1,17 | 0,34 |
| 111 | 1,45 | 0,32 | 2,43 | 0,51 | 1,46 | 0,38 |
| 113 | 1,80 | 0,35 | 0,95 | 0,32 | 1,56 | 0,39 |
| 115 | 1,04 | 0,27 | 0,95 | 0,32 | 0,58 | 0,24 |
| 117 | 0,83 | 0,24 | 0,63 | 0,26 | 0,49 | 0,22 |
| 119 | 0,48 | 0,18 | 0,42 | 0,21 | 0,49 | 0,22 |
| 121 | 0,76 | 0,23 | 0,42 | 0,21 | 0,58 | 0,24 |
| 123 | 0,55 | 0,20 | 0,42 | 0,21 | 0,68 | 0,26 |
| 125 | 0,76 | 0,23 | 0,42 | 0,21 | 0,58 | 0,24 |
| 127 | 0,35 | 0,15 | 0,74 | 0,28 | 0,78 | 0,28 |
| 129 | 0,76 | 0,23 | 0,85 | 0,30 | 1,85 | 0,42 |
| 131 | 1,45 | 0,32 | 1,06 | 0,33 | 1,66 | 0,40 |
| 133 | 1,66 | 0,34 | 0,95 | 0,32 | 1,46 | 0,38 |
| 135 | 2,00 | 0,37 | 2,33 | 0,50 | 2,43 | 0,49 |
| 137 | 2,76 | 0,44 | 2,43 | 0,51 | 2,92 | 0,53 |
| 139 | 3,73 | 0,51 | 3,70 | 0,63 | 3,31 | 0,57 |
| 141 | 2,76 | 0,44 | 3,28 | 0,59 | 3,80 | 0,61 |
| 143 | 3,94 | 0,52 | 3,60 | 0,62 | 2,73 | 0,52 |
| 145 | 3,18 | 0,47 | 3,28 | 0,59 | 3,02 | 0,54 |
| 147 | 3,45 | 0,49 | 3,70 | 0,63 | 3,51 | 0,58 |
| 149 | 2,90 | 0,45 | 3,28 | 0,59 | 3,99 | 0,62 |
| 151 | 3,11 | 0,46 | 2,86 | 0,55 | 3,80 | 0,61 |
| 153 | 2,62 | 0,43 | 2,22 | 0,48 | 3,41 | 0,58 |
| 155 | 2,14 | 0,38 | 1,59 | 0,41 | 2,82 | 0,52 |
| 157 | 2,49 | 0,41 | 2,01 | 0,46 | 2,14 | 0,46 |
| 159 | 1,17 | 0,28 | 1,80 | 0,44 | 1,85 | 0,42 |
| 161 | 1,24 | 0,29 | 0,85 | 0,30 | 2,04 | 0,45 |
| 163 | 0,97 | 0,26 | 1,48 | 0,40 | 1,27 | 0,35 |
| 165 | 1,04 | 0,27 | 1,27 | 0,37 | 1,75 | 0,41 |
| 167 | 0,83 | 0,24 | 0,85 | 0,30 | 1,27 | 0,35 |
| 169 | 0,62 | 0,21 | 0,53 | 0,24 | 0,97 | 0,31 |
| 171 | 0,35 | 0,15 | 0,11 | 0,11 | 0,49 | 0,22 |
| 173 | 0,21 | 0,12 | 0,42 | 0,21 | 0,29 | 0,17 |
| 175 | 0,41 | 0,17 | 0,32 | 0,18 | 0,19 | 0,14 |
| 177 | 0,07 | 0,07 | 0,11 | 0,11 | 0,29 | 0,17 |
| 179 | 0,00 | 0,00 | 0,11 | 0,11 | 0,00 | 0,00 |
| 181 | 0,07 | 0,07 | 0,00 | 0,00 | 0,10 | 0,10 |
| 183 | 0,07 | 0,07 | 0,00 | 0,00 | 0,10 | 0,10 |
| 185 | 0,00 | 0,00 | 0,11 | 0,11 | 0,19 | 0,14 |
| 187 | 0,07 | 0,07 | 0,00 | 0,00 | 0,10 | 0,10 |
| 189 | 0,00 | 0,00 | 0,11 | 0,11 | 0,00 | 0,00 |

Tab. B Preliminary ^{235}U mass yields for incident neutron energies of 8,10 and 12 MeV.

See text for details.

| Energy (MeV) | En = 8 MeV | | En = 10 MeV | | En = 12 MeV | |
|-----------------|---------------|--------|---------------|--------|---------------|--------|
| | Yields (a.u.) | Errors | Yields (a.u.) | Errors | Yields (a.u.) | Errors |
| 65 | 0,06 | 0,06 | 0,05 | 0,05 | 0,00 | 0,00 |
| 67 | 0,18 | 0,11 | 0,00 | 0,00 | 0,13 | 0,07 |
| 69 | 0,06 | 0,06 | 0,00 | 0,00 | 0,13 | 0,07 |
| 71 | 0,06 | 0,06 | 0,05 | 0,05 | 0,00 | 0,00 |
| 73 | 0,30 | 0,14 | 0,05 | 0,05 | 0,08 | 0,06 |
| 75 | 0,06 | 0,06 | 0,26 | 0,12 | 0,17 | 0,08 |
| 77 | 0,43 | 0,16 | 0,26 | 0,12 | 0,25 | 0,10 |
| 79 | 0,61 | 0,19 | 0,47 | 0,16 | 0,42 | 0,13 |
| 81 | 0,73 | 0,21 | 0,67 | 0,19 | 0,59 | 0,16 |
| 83 | 1,22 | 0,27 | 0,88 | 0,21 | 1,01 | 0,21 |
| 85 | 1,52 | 0,30 | 1,71 | 0,30 | 1,64 | 0,26 |
| 87 | 2,19 | 0,36 | 2,49 | 0,36 | 1,77 | 0,27 |
| 89 | 2,31 | 0,37 | 2,23 | 0,34 | 2,40 | 0,32 |
| 91 | 2,92 | 0,42 | 3,16 | 0,41 | 2,40 | 0,32 |
| 93 | 3,04 | 0,43 | 3,48 | 0,42 | 3,16 | 0,36 |
| 95 | 4,62 | 0,53 | 3,63 | 0,43 | 2,95 | 0,35 |
| 97 | 4,13 | 0,50 | 3,42 | 0,42 | 3,12 | 0,36 |
| 99 | 4,32 | 0,51 | 3,37 | 0,42 | 2,99 | 0,36 |
| 101 | 4,32 | 0,51 | 3,94 | 0,45 | 2,87 | 0,35 |
| 103 | 3,34 | 0,45 | 3,63 | 0,43 | 3,33 | 0,37 |
| 105 | 2,67 | 0,40 | 2,54 | 0,36 | 2,36 | 0,32 |
| 107 | 2,07 | 0,35 | 2,18 | 0,34 | 1,35 | 0,24 |
| 109 | 1,58 | 0,31 | 1,40 | 0,27 | 1,73 | 0,27 |
| 111 | 0,97 | 0,24 | 0,99 | 0,23 | 1,69 | 0,27 |
| 113 | 1,03 | 0,25 | 1,24 | 0,25 | 1,14 | 0,22 |
| 115 | 0,55 | 0,18 | 0,93 | 0,22 | 1,22 | 0,23 |
| 117 | 0,67 | 0,20 | 0,73 | 0,19 | 0,88 | 0,19 |
| 119 | 0,36 | 0,15 | 0,93 | 0,22 | 1,01 | 0,21 |
| 121 | 0,85 | 0,23 | 1,14 | 0,24 | 1,26 | 0,23 |
| 123 | 0,73 | 0,21 | 1,04 | 0,23 | 0,93 | 0,20 |
| 125 | 0,85 | 0,23 | 0,83 | 0,21 | 1,26 | 0,23 |
| 127 | 0,91 | 0,24 | 1,66 | 0,29 | 1,35 | 0,24 |
| 129 | 0,91 | 0,24 | 1,40 | 0,27 | 0,88 | 0,19 |
| 131 | 1,64 | 0,32 | 2,02 | 0,32 | 1,77 | 0,27 |
| 133 | 1,88 | 0,34 | 1,71 | 0,30 | 2,23 | 0,31 |
| 135 | 2,49 | 0,39 | 1,92 | 0,32 | 2,95 | 0,35 |
| 137 | 2,86 | 0,42 | 2,70 | 0,37 | 2,40 | 0,32 |
| 139 | 3,59 | 0,47 | 3,68 | 0,44 | 3,24 | 0,37 |
| 141 | 3,83 | 0,48 | 3,89 | 0,45 | 4,09 | 0,42 |
| 143 | 3,16 | 0,44 | 3,42 | 0,42 | 4,47 | 0,43 |
| 145 | 3,22 | 0,44 | 3,84 | 0,45 | 3,79 | 0,40 |
| 147 | 3,34 | 0,45 | 3,42 | 0,42 | 3,41 | 0,38 |
| 149 | 4,26 | 0,51 | 3,37 | 0,42 | 3,08 | 0,36 |
| 151 | 3,34 | 0,45 | 2,70 | 0,37 | 3,29 | 0,37 |
| 153 | 2,31 | 0,37 | 2,23 | 0,34 | 2,95 | 0,35 |
| 155 | 2,25 | 0,37 | 2,44 | 0,36 | 2,91 | 0,35 |
| 157 | 2,31 | 0,37 | 2,18 | 0,34 | 2,19 | 0,30 |
| 159 | 1,64 | 0,32 | 1,92 | 0,32 | 1,90 | 0,28 |
| 161 | 1,58 | 0,31 | 1,30 | 0,26 | 1,39 | 0,24 |
| 163 | 1,28 | 0,28 | 1,09 | 0,24 | 1,64 | 0,26 |
| 165 | 1,09 | 0,26 | 0,73 | 0,19 | 1,14 | 0,22 |
| 167 | 0,91 | 0,24 | 1,04 | 0,23 | 1,26 | 0,23 |
| 169 | 0,73 | 0,21 | 0,73 | 0,19 | 0,72 | 0,17 |
| 171 | 0,36 | 0,15 | 0,57 | 0,17 | 0,42 | 0,13 |
| 173 | 0,36 | 0,15 | 0,67 | 0,19 | 0,63 | 0,16 |
| 175 | 0,24 | 0,12 | 0,47 | 0,16 | 0,29 | 0,11 |
| 177 | 0,06 | 0,06 | 0,21 | 0,10 | 0,42 | 0,13 |
| 179 | 0,30 | 0,14 | 0,21 | 0,10 | 0,25 | 0,10 |
| 181 | 0,00 | 0,00 | 0,10 | 0,07 | 0,21 | 0,09 |
| 183 | 0,18 | 0,11 | 0,10 | 0,07 | 0,04 | 0,04 |
| 185 | 0,06 | 0,06 | 0,00 | 0,00 | 0,00 | 0,00 |
| 187 | 0,00 | 0,00 | 0,16 | 0,09 | 0,17 | 0,08 |
| 189 | 0,00 | 0,00 | 0,10 | 0,07 | 0,00 | 0,00 |
| 191 | 0,06 | 0,06 | 0,00 | 0,00 | 0,04 | 0,04 |

Tab. C Preliminary ^{235}U mass yields for incident neutron energies of 14, 16 and 18 MeV.
See text for details.

| Energy (MeV) | En = 8 MeV | | En = 10 MeV | | En = 12 MeV | |
|-----------------|---------------|--------|---------------|--------|---------------|--------|
| | Yields (a.u.) | Errors | Yields (a.u.) | Errors | Yields (a.u.) | Errors |
| 67 | 0,14 | 0,07 | 0,09 | 0,05 | 0,13 | 0,07 |
| 69 | 0,03 | 0,03 | 0,03 | 0,03 | 0,10 | 0,06 |
| 71 | 0,10 | 0,06 | 0,12 | 0,06 | 0,10 | 0,06 |
| 73 | 0,07 | 0,05 | 0,12 | 0,06 | 0,07 | 0,05 |
| 75 | 0,28 | 0,10 | 0,21 | 0,08 | 0,30 | 0,10 |
| 77 | 0,24 | 0,09 | 0,31 | 0,10 | 0,36 | 0,11 |
| 79 | 0,24 | 0,09 | 0,46 | 0,12 | 0,83 | 0,17 |
| 81 | 0,65 | 0,15 | 0,58 | 0,13 | 0,90 | 0,17 |
| 83 | 0,90 | 0,18 | 1,17 | 0,19 | 1,03 | 0,18 |
| 85 | 1,14 | 0,20 | 2,03 | 0,25 | 1,99 | 0,26 |
| 87 | 1,52 | 0,23 | 2,03 | 0,25 | 2,55 | 0,29 |
| 89 | 1,96 | 0,26 | 2,36 | 0,27 | 2,95 | 0,31 |
| 91 | 2,03 | 0,26 | 2,49 | 0,28 | 3,55 | 0,34 |
| 93 | 2,82 | 0,31 | 3,65 | 0,34 | 3,58 | 0,34 |
| 95 | 3,51 | 0,35 | 4,21 | 0,36 | 4,05 | 0,37 |
| 97 | 2,96 | 0,32 | 4,15 | 0,36 | 4,08 | 0,37 |
| 99 | 3,41 | 0,34 | 3,26 | 0,32 | 3,88 | 0,36 |
| 101 | 3,48 | 0,35 | 3,38 | 0,32 | 3,25 | 0,33 |
| 103 | 3,13 | 0,33 | 2,98 | 0,30 | 3,68 | 0,35 |
| 105 | 2,24 | 0,28 | 3,04 | 0,31 | 2,69 | 0,30 |
| 107 | 1,55 | 0,23 | 2,40 | 0,27 | 1,96 | 0,25 |
| 109 | 1,62 | 0,24 | 1,97 | 0,25 | 1,53 | 0,22 |
| 111 | 1,38 | 0,22 | 1,60 | 0,22 | 2,02 | 0,26 |
| 113 | 1,79 | 0,25 | 1,07 | 0,18 | 1,36 | 0,21 |
| 115 | 1,24 | 0,21 | 1,17 | 0,19 | 1,72 | 0,24 |
| 117 | 1,45 | 0,22 | 0,89 | 0,17 | 1,29 | 0,21 |
| 119 | 0,96 | 0,18 | 1,17 | 0,19 | 1,86 | 0,25 |
| 121 | 1,55 | 0,23 | 1,17 | 0,19 | 1,43 | 0,22 |
| 123 | 1,45 | 0,22 | 2,00 | 0,25 | 1,63 | 0,23 |
| 125 | 1,14 | 0,20 | 1,57 | 0,22 | 1,66 | 0,23 |
| 127 | 1,27 | 0,21 | 1,50 | 0,21 | 1,39 | 0,21 |
| 129 | 2,31 | 0,28 | 1,20 | 0,19 | 2,22 | 0,27 |
| 131 | 1,69 | 0,24 | 2,00 | 0,25 | 2,35 | 0,28 |
| 133 | 2,41 | 0,29 | 2,64 | 0,28 | 1,59 | 0,23 |
| 135 | 2,79 | 0,31 | 2,15 | 0,26 | 2,12 | 0,27 |
| 137 | 2,89 | 0,32 | 2,86 | 0,30 | 2,89 | 0,31 |
| 139 | 3,48 | 0,35 | 3,41 | 0,32 | 2,95 | 0,31 |
| 141 | 4,62 | 0,40 | 3,26 | 0,32 | 2,95 | 0,31 |
| 143 | 3,93 | 0,37 | 3,81 | 0,34 | 2,69 | 0,30 |
| 145 | 3,48 | 0,35 | 3,29 | 0,32 | 3,25 | 0,33 |
| 147 | 3,65 | 0,35 | 3,22 | 0,31 | 2,49 | 0,29 |
| 149 | 3,65 | 0,35 | 2,52 | 0,28 | 2,65 | 0,30 |
| 151 | 2,96 | 0,32 | 3,01 | 0,30 | 2,12 | 0,27 |
| 153 | 3,00 | 0,32 | 2,43 | 0,27 | 2,49 | 0,29 |
| 155 | 2,48 | 0,29 | 1,90 | 0,24 | 2,19 | 0,27 |
| 157 | 1,86 | 0,25 | 2,00 | 0,25 | 1,36 | 0,21 |
| 159 | 1,55 | 0,23 | 1,50 | 0,21 | 0,96 | 0,18 |
| 161 | 1,55 | 0,23 | 1,07 | 0,18 | 0,93 | 0,18 |
| 163 | 1,03 | 0,19 | 0,77 | 0,15 | 0,80 | 0,16 |
| 165 | 1,10 | 0,19 | 0,71 | 0,15 | 0,80 | 0,16 |
| 167 | 0,62 | 0,15 | 0,95 | 0,17 | 0,60 | 0,14 |
| 169 | 0,79 | 0,17 | 0,52 | 0,13 | 0,50 | 0,13 |
| 171 | 0,41 | 0,12 | 0,37 | 0,11 | 0,33 | 0,10 |
| 173 | 0,31 | 0,10 | 0,37 | 0,11 | 0,20 | 0,08 |
| 175 | 0,14 | 0,07 | 0,25 | 0,09 | 0,13 | 0,07 |
| 177 | 0,28 | 0,10 | 0,25 | 0,09 | 0,10 | 0,06 |
| 179 | 0,07 | 0,05 | 0,12 | 0,06 | 0,03 | 0,03 |
| 181 | 0,17 | 0,08 | 0,06 | 0,04 | 0,07 | 0,05 |
| 183 | 0,07 | 0,05 | 0,03 | 0,03 | 0,07 | 0,05 |
| 185 | 0,14 | 0,07 | 0,03 | 0,03 | 0,03 | 0,03 |
| 187 | 0,07 | 0,05 | 0,00 | 0,00 | 0,00 | 0,00 |
| 189 | 0,03 | 0,03 | 0,06 | 0,04 | 0,00 | 0,00 |